Copper-induced Recrystallization and Interdiffusion of CdTe/ZnTe Thin Films

Running title: Copper-induced Recrystallization and Interdiffusion of CdTe/ZnTe Thin Films

Running Authors: Samoilenko et al.

Yegor Samoilenko, Colin A. Wolden[a)]

Department of Chemical and Biological Engineering, Colorado School of Mines, Golden, CO 80401, USA

Ali Abbas, J. Michael Walls

CREST, Wolfson School of Mechanical, Electrical and Manufacturing Engineering, Loughborough University, Loughborough LE11 3TU, UK

[a)] Electronic mail: cwolden@mines.edu

ZnTe is commonly employed as a buffer layer between CdTe and the metallization layer at the back contact of state-of-the-art CdTe solar cells. Here the critical role of Cu in catalyzing recrystallization and interdiffusion between CdTe and ZnTe layers during back contact activation is presented. Several CdTe/ZnTe:Cu thin-film samples were prepared with varying levels of copper loading and annealed as a function of temperature and time. The samples were characterized by x-ray diffractometry, scanning electron microscopy, transmission electron microscopy, and energy dispersive x-ray spectroscopy. The results show that stress is present in the as-deposited bilayers and that negligible interdiffusion occurs in the absence of Cu. The presence of Cu facilitates rapid interdiffusion, predominantly via Cd migration into the ZnTe phase. Zn migration into CdTe is limited to areas around defects and grain boundaries. Ternary $Cd_xZn_{1-x}Te$ interlayers are formed, and the extent of alloy formation ranges from $0.08 < x < 0.5$ throughout the whole ZnTe

layer. The level of Cu loading controls the composition of the Cu_xTe clusters observed, while their size and migration is a function of annealing conditions.

I. INTRODUCTION

Cadmium telluride (CdTe) has emerged as the leading thin-film photovoltaic (PV) technology and is poised to reach grid parity soon with record device efficiency currently at 22.1%.[1] A long-standing challenge in this technology is making good ohmic contact with CdTe, which is challenging due to its low doping and high work function. A common strategy to address this problem is through the insertion of a thin interfacial layer between the CdTe and metal contact.[2] Copper-doped zinc telluride (ZnTe:Cu) has been widely adopted for this role.[3] Copper degenerately dopes this layer, which narrows the barrier width and permits electron tunneling, creating a quasi-ohmic contact.[4] First Solar Inc. has integrated ZnTe buffer layers into their commercial modules,[5] crediting this change with improving champion device efficiency as well as enhancing both the stability and temperature sensitivity of their modules.

Copper appears to be essential for achieving high efficiency devices, but it has also been implicated with several defect states located within the CdTe band gap.[6] Cu can rapidly diffuse via grain boundaries into the bulk CdTe and to the front contact interface. This creates recombination centers and/or shunting pathways which have a negative effect on the efficiency of the devices. Copper migration has also been implicated in contributing to problems with stability.[7] In conventional device fabrication ZnTe:Cu is deposited on CdTe and subjected to thermal activation. We recently introduced rapid

thermal processing (RTP) as a high throughput approach to deliver precise control over this process.[8] For devices contacted with a gold metallization layer, it was shown that the majority of Cu either alloyed with the gold or it became sequestered in core-shell clusters of $Cu_{1.4}Te$ surrounded by Zn.[9] Another observation was that significant CdTe-ZnTe interdiffusion can occur over these short time scales and may be an important contributor to the high fill factor and open circuit voltages observed.[10] In this paper, we explore this latter process in more detail as a function of copper loading, time, and temperature. It is shown that the presence of Cu is essential for any significant interdiffusion to occur, not unlike the role of $CdCl_2$ promoting CdS/CdTe interdiffusion at the front contact.[11] In addition, it is found that excess Te in the as-deposited ZnTe layers and morphology are important factors that contribute to the degree of interdiffusion observed.

II. EXPERIMENTAL

CdTe of ~4 um thickness was deposited by Vapor Transport Deposition (VTD) on pre-cleaned 1.5" x 1.5" TEC15 superstrates obtained from Hartford Glass. CdTe source and substrate were held at 620 and 420 ºC, respectively. Following CdTe deposition, devices underwent $CdCl_2$ treatment at T = 405 ºC for 30 min under 50/50 vol% mixture of N_2 and O_2. $CdCl_2$ treated devices were etched for 10 seconds in 0.5 vol% bromine/methanol mixture and rinsed for 60 seconds in methanol to create a Te-rich layer on top of the CdTe. ZnTe and Cu were co-evaporated inside the thermal evaporator with the substrate held at 100^{o}C. The thickness of ZnTe was kept at ~1 µm and Cu thicknesses were varied between 0 and 86 nm to get approximately 0, 3, 5.5, and 8 vol% Cu loading in ZnTe. The ZnTe thickness was chosen to provide good resolution of both the CdTe and ZnTe layers in subsequent characterization. Deposition rate and thicknesses were

controlled and measured by quartz crystal monitors. The final step was the heat treatment inside the rapid thermal processing (RTP) chamber under N_2 atmosphere at 2.5 Torr. During this step the samples were rapidly (20 seconds) heated to a set temperature and held at that temperature for a specified time. X-ray diffraction (XRD) was used to analyze the crystal structure of the films and to track the extent of interdiffusion. The step size was 0.05^o with a dwell time of 1 second. Transmission Electron Microscopy (TEM) was the tool used to investigate the detailed microstructure of these bilayers. TEM samples were prepared by focused ion beam (FIB) milling using a dual beam FEI Nova 600 nanolab. A standard *in situ* lift out method described previously was employed for sample preparation.[12] TEM imaging was carried out in a FEI Tecnai F20 equipped with an Oxford Instruments X-Max 80 silicon drift detector (SDD) energy dispersive X-ray detector (EDX). EDX was used to produce chemical distribution maps of the cells as well as line scans and point analysis for quantitative elemental analysis. Cross-sectional TEM along with energy dispersive X-ray analysis (EDAX) was employed to investigate the cross sections of the devices and map elemental compositions.

The effects of three parameters on the interdiffusion between CdTe and ZnTe layers were studied: temperature, time, and Cu loading. The list below shows the studied conditions:

- Temperature: 320, 340, and 360 ºC
- Cumulative time: 30, 120, 300 seconds
- Copper Loading: 0, 3, 5.5, 8 vol%

The lower values are most representative of what is used in device processing, with optimal performance employing RTP annealing conditions of 320-340 ºC for 60-120

s.[8] In addition, the buffer layer thickness used in devices is ~165 nm. The use of thicker films and greater times/temperatures in this work facilitated characterization of the trends observed. The Cu loadings were chosen to span the range of Cu content that have yielded optimal solar cell performance in our lab. The highest loading corresponds to Au-contacted devices, with decreasing loadings corresponding to Ti and Cr-contacted devices, respectively.[13] In the case of Cu-miscible contacts such as gold, the majority of copper alloys with the metal contact that is not present in the current study. Thus, the 3% loading is most representative of copper availability within ZnTe under device conditions, but again the use of larger amounts was useful for characterization and trend analysis.

III. RESULTS AND DISCUSSION

A. As-deposited vs. Fully Annealed Comparison

To provide an overview of the major observations we begin with a comparison of as-deposited films with those fully annealed at the highest temperature and longest time (360 ºC/5 minutes). A more detailed and quantitative evaluation of the impact of individual parameters is presented in the subsequent sections. Figure 1 compares the XRD patterns obtained from as-deposited bilayers and after full annealing as a function of copper loading. As-deposited samples with 0 and 3% Cu only display peaks associated with CdTe and ZnTe. The CdTe XRD pattern displays the random grain orientation expected for $CdCl_2$ treated samples.[14] Minor peaks associated with Cu_xTe phases are observed in as-deposited films at the two higher Cu loading levels.

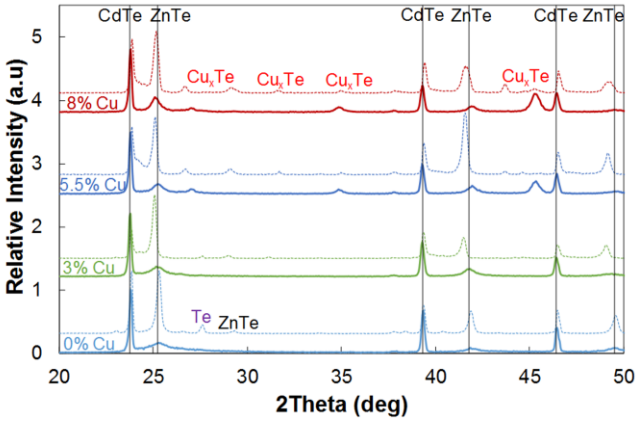

FIG. 1 (Color Online). XRD patterns of CdTe|ZnTe bilayers obtained from as-deposited films (solid lines) and after full annealing (T = 360 ºC, t= 5 min, dashed lines) as a function of copper loading.

There are several important differences that can be observed upon annealing. First, in the absence of Cu, there is negligible CdTe|ZnTe interdiffusion or alloy formation. Annealing improves ZnTe crystallinity as evidenced by the increased intensity, but there is no shift in peak position. In contrast, significant interdiffusion is observed at all levels of Cu loading. Thus, it appears that the presence of Cu is essential to promote significant interdiffusion at these conditions. Second, the extent of ZnTe peak shift is more pronounced compared to CdTe peaks. This suggests that alloy formation primarily reflects incorporation of Cd into the ZnTe lattice rather than Zn into CdTe. Although both CdTe and ZnTe peaks are sharp, the region between them is well above the background levels suggesting the presence of a significant interlayer of varying composition. Confirmation of these findings is provided by elemental mapping, which are provided for fully annealed samples at the 0 and 3% Cu loading levels in Figure 2. Both the Zn and the Cd density profiles are abruptly attenuated at the CdTe|ZnTe interface in the 0% sample. In contrast, a diffuse interface is observed in the 3% Cu

sample, with significant amounts of Cd detected throughout the ZnTe layer. Quantification of these phenomena is presented in the Section III.B below.

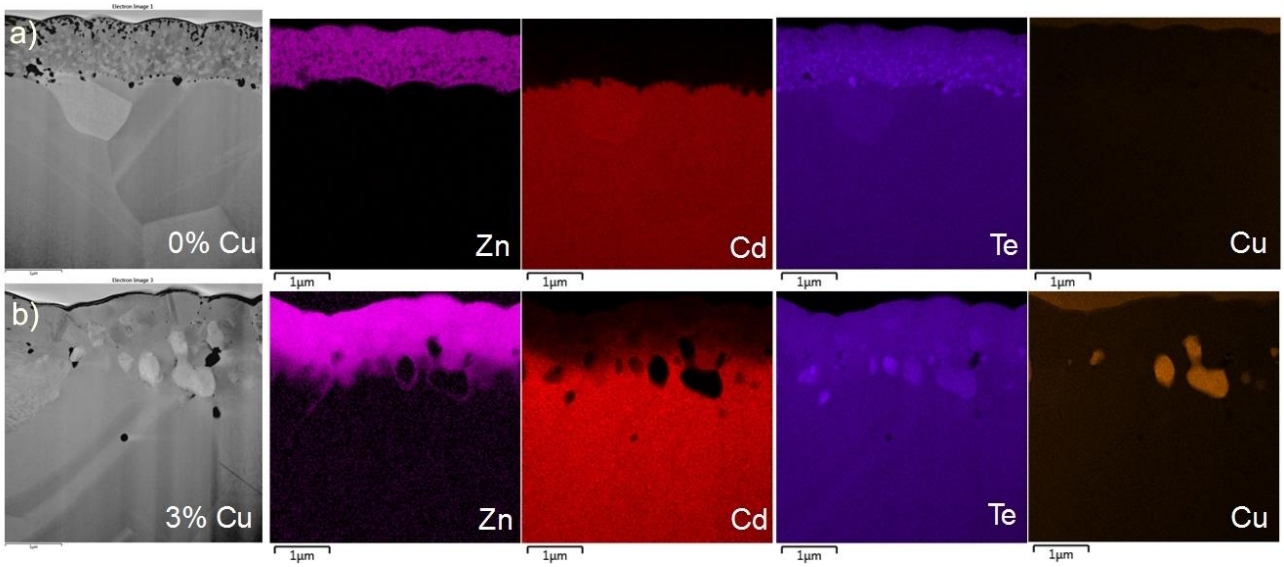

FIG. 2 (Color Online). Comparison of TEM images and elemental EDAX maps after annealing at T = 360 ºC for a cumulative time of t = 5 min: a) 0 % Cu; b) 3% Cu.

The presence of Cu was also observed to have a major impact on the morphology of the ZnTe layer. In the absence of Cu this layer retains a nanocrystalline morphology, and the presence of excess Te in the form of nanoclusters that are detected by both XRD and EDAX mapping. EDAX measurements of as-deposited ZnTe:Cu on glass confirm the presence of excess Te, which is consistent with previous reports of ZnTe films prepared by physical vapor deposition.[15,16,17] The absence of a Te peak in the as-deposited XRD suggests that it is present in an amorphous form, whereas it crystallizes and clusters upon annealing (Figs. 1, 2). Another potential contributor to excess Te may be some degree of preferential evaporation of Zn during annealing. The presence of Cu also facilitates ZnTe crystal growth as all annealed films containing Cu displayed ZnTe layers consisting of large, well-defined grains that are largely free of the voids and defects observed in the absence of Cu. Copper, which is distributed uniformly in as-

deposited ZnTe, scavenges excess Te (Fig. 1) to form Cu_xTe, which aggregates into well-defined clusters (Fig. 2). The size, composition, and migration of these clusters is a strong function of time, temperature, and copper loading as discussed in Section III.C below.

B. Interdiffusion and Alloy Formation

The degree of interdiffusion and alloy formation was quantified by XRD analysis and EDAX profiling. Figure 1 displayed XRD evolution as a function of Cu loading, and Figure 3 displays XRD patterns obtained as a function of both annealing time and temperature for the intermediate 5.5% Cu sample. Additional patterns for the complete set of conditions examined are provided in the Supplemental Information (Figs. S1, S2, S3). There are a number of qualitative trends that may be observed. First, as–deposited ZnTe films have poor crystallinity, but the peak intensity and width are increased and reduced, respectively, with increasing annealing time and/or temperature. In addition, the ZnTe peak position shifts to lower values of 2θ due to cadmium substitution. In contrast, the CdTe peak position remains largely unchanged, and its intensity is attenuated reflecting the improvement in ZnTe crystal quality. Finally, the intensity of the diffraction signal between the distinct CdTe and ZnTe peaks increases with time and temperature, reflecting the presence and growth of a graded $Cd_xZn_{1-x}Te$ alloy. This "diffusion tail", linking CdTe and ZnTe peaks can be attributed to variations of alloy compositions at the grain boundaries vs. bulk due to the difference in diffusivities. Similarly to a plot of sulfur distribution in CdTe shown by McCandless et. al.,[18] $Cd_xZn_{1-x}Te$ concentration throughout ZnTe grains will vary from high to low x values as we move from grain boundary to the grain interior. This can be partially seen in the TEM

EDAX maps. The difference in alloy concentration would be more pronounced in ZnTe with larger grains. The more pronounced "diffusion tails" in (111) peaks in Figure 1 of 5.5% and 8% Cu samples is consistent with the effect of Cu on ZnTe grain size that will be discussed in more detail in Section III.C. below (see Fig. 10).

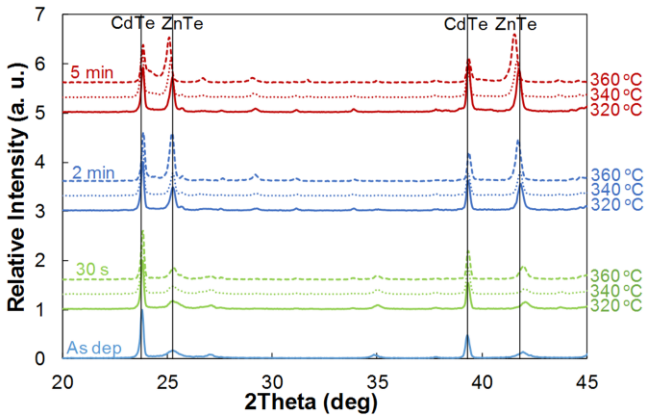

FIG. 3 (Color Online). XRD patterns from the 5.5 vol% Cu sample annealed at 320, 340, and 360 ^{o}C after 0.5, 2, and 5 minutes of cumulative annealing.

Vegard's Law was used to calculate the composition of $Cd_xZn_{1-x}Te$ alloy formed during annealing based on the ZnTe (220) peak position ($2\theta = 25.26^{o}$). The resulting alloy compositions are shown in Figure 4 as a function of annealing time, temperature and copper loading. The compositions extracted from as-deposited films were non-zero, with negative values attributed to the presence of compressive stress, and conversely positive values reflect tensile stress. Rakhshani also reported the presence of stress in ZnTe films deposited at temperatures below 305 ^{o}C.[19] The apparent "reduction" in alloy composition after the first 30 s treatment is attributed predominantly to the release of stress present in the as-deposited films, which overshadows any compositional changes. For copper–free bilayers, the value remains largely unchanged and near zero for all times and temperatures, as one would expect for the case of negligible interdiffusion. For ZnTe

films containing copper the extracted value of x increased monotonically with both annealing time and annealing temperature. Final cadmium fractions ranged from x ~ 0.03 at T = 320 ºC to x ~ 0.16 at T = 360 ºC.

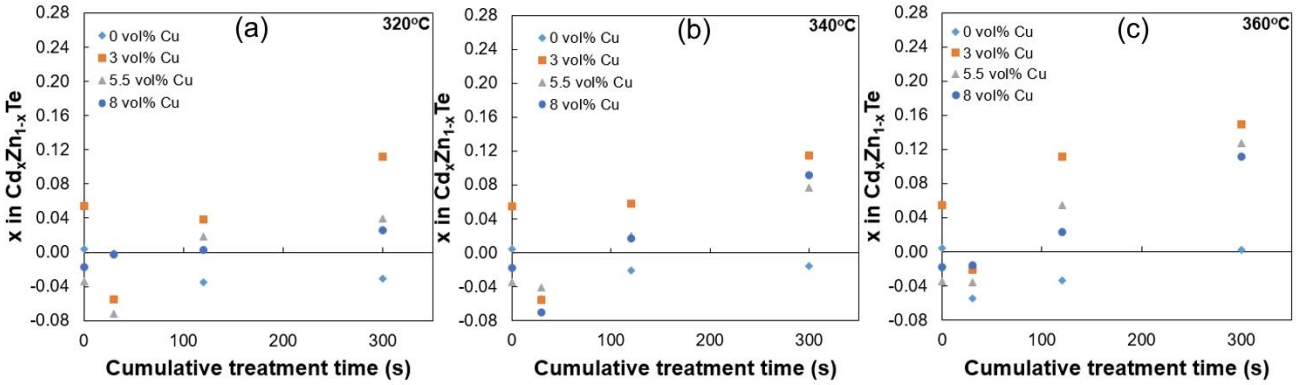

FIG. 4 (Color Online). $Cd_xZn_{1-x}Te$ alloy composition as function of annealing time, Cu loading, and annealing temperature based on analysis of the ZnTe (220) peak position: a) 320 ºC; b) 340 ºC; c) 360 ºC.

Arrhenius plots were constructed based on the alloy compositions of samples annealed for 5 min and are shown in Figure 5. Activation energies were calculated from the fit and came out to 0.23, 0.94, and 1.19 eV for 3, 5.5, and 8% Cu samples, respectively. These values are significantly lower than values of Cd and Zn self-diffusion in CdTe and ZnTe at 2.67 eV and 2.69 eV, respectively.[20,21] Borsenberger et. al.[20] saw self-diffusion of Cd accelerate when Al was introduced into CdTe, with activation energy dropping to 0.67 eV. Similarly, it seems Cu has an analogous effect, triggering diffusion of Cd through CdTe into ZnTe film. Interestingly, reported activation energy for Cu diffusion in CdTe is 0.33-0.67 eV,[22-24] which is in the ballpark of activation energies found for 3 and 5.5% Cu samples.

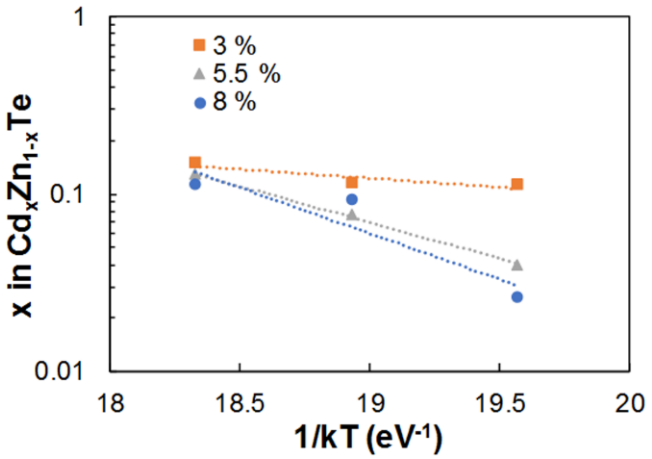

FIG. 5 (Color Online). Arrhenius plot of $Cd_xZn_{1-x}Te$ alloy compositions based on analysis of the ZnTe (220) peak position of samples annealed for 5 min.

Interestingly, in all cases the most substantial degree of alloying was observed for the lowest copper loading (3%), with the difference being more pronounced at lower temperature and/or time. To better understand the dependence on copper concentration compositional profiling was performed on TEM samples. Figures 6 & 7 show the Cd and Zn concentration data extracted from EDAX line and area scans obtained from samples after annealing at T = 360 ºC for 5 minutes. For clarity, we compare the results at low and high Cu loading (3 vs. 8%). Fig. 6 plots line scans of the Cd and Zn concentration starting in the bulk CdTe and continuing through the entirety of the ZnTe layer. Both profiles were aligned relative to a common "interface" position, defined as the Zn=Cd crossover position. The profiles behave monotonically, with the exceptions of bumps which are artifacts introduced by the presence of the Cu_xTe clusters. Consistent with the XRD analysis it is found that the degree of interdiffusion is much more extensive for the 3% sample. In the 3% sample there is a nominally linear gradient in Cd that begins at about ~1.5 microns deep in the CdTe layer and extends throughout the full ZnTe layer, reaching a final value of x ~0.1 deep within the ZnTe layer. Zn diffusion also extends

almost a micron into the CdTe at 3% Cu loading. For the 8% Cu loading, the Cd gradient is limited to a few hundred nm either side of the interface, but the Cd concentration extends throughout the ZnTe layer at a saturated value of x~0.04. The degree of Zn diffusion is also greatly attenuated in the 8% sample.

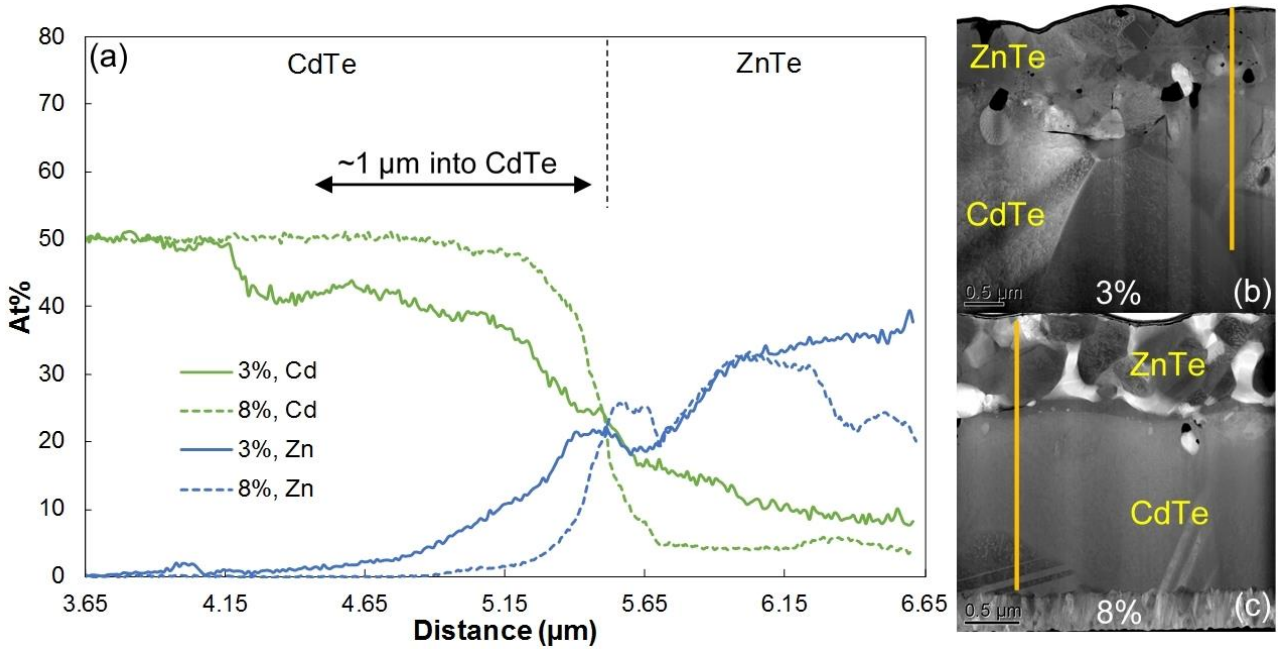

FIG. 6 (Color Online). a) Cd and Zn profiles from EDAX line scans in 3% and 8% samples annealed at 360 ^{o}C for 5 min; b) line scan position for 3% Cu sample; c) line scan position for 8% Cu sample.

There is a significant degree of heterogeneity in these samples, so to provide more representative measurements the degree of interdiffusion was quantified in two different ways. Figure 7b shows the atomic concentration of Zn in CdTe and Cd in ZnTe obtained by averaging line scans such as those in Fig. 6. These finding confirm that the degree of interdiffusion increases as the Cu loading is reduced, and the values of Cd in ZnTe are consistent with the composition values extracted from the XRD Vegard analysis (Fig. 4). The second approach was based on area scans performed within both the ZnTe and CdTe layers from the regions highlighted in Figure 7a. These regions were chosen as they

appear relatively homogenous and they were located far from Cu_xTe clusters that can significantly perturb the measurements. The average concentrations obtained from these regions are shown in Figure 7c. The values for Cd in ZnTe are consistent with Fig. 7b with respect to both the absolute value and the trend with Cu loading. The slightly lower values reflect the fact that these regions are somewhat removed from the interface where the Cd density is greater. In contrast, essentially no Zn is detected within the relatively large CdTe regions selected for analysis. This observation is consistent with the negligible shift in the CdTe peak position observed in all the XRD patterns.

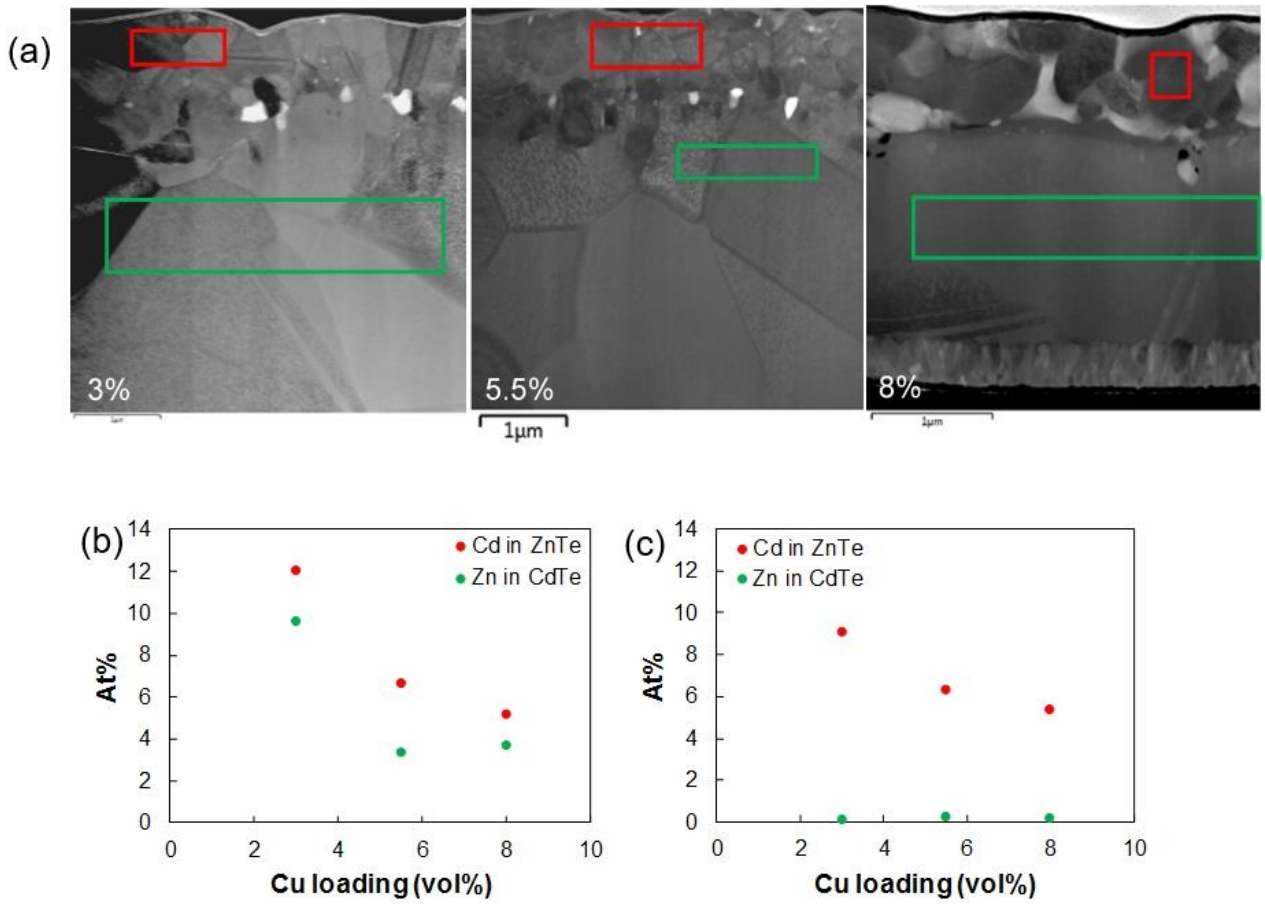

FIG. 7 (Color Online). a) TEM images with the region of area scans highlighted; b) average concentrations of Cd in 1 micron of ZnTe layer and Zn in 1 micron of CdTe

calculated from EDAX line scans; c) concentrations of Cd and Zn obtained from the selected area scans shown in (a).

The apparent discrepancy in Figures 7b,c is explained and reconciled by considering the important role of morphology on cation exchange. As deposited ZnTe films are nanocrystalline and defective, and Cd diffusion into the ZnTe layer is observed to proceed largely in a uniform fashion. In contrast, the CdTe layers consist of large, well crystallized grains that are produced during the $CdCl_2$ step. It is observed that Zn diffusion is limited primarily to regions that contain defects such as grain boundaries or Cu_xTe clusters. To illustrate the important role of morphology Figure 8 compares TEM images and elemental mapping from two regions of the same sample (fully annealed 8% Cu). Image A is from a region containing numerous Cu_xTe clusters near the interface, while image B is from a clean interfacial region containing a single small Cu_xTe cluster. As clearly shown in the elemental mapping significant amounts of Zn are observed within the CdTe layer in the outlined regions where Cu_xTe clusters are present, whereas only slight movement is observed in the absence of such defects. Zn migration into the CdTe is significantly attenuated in the absence of such defects.

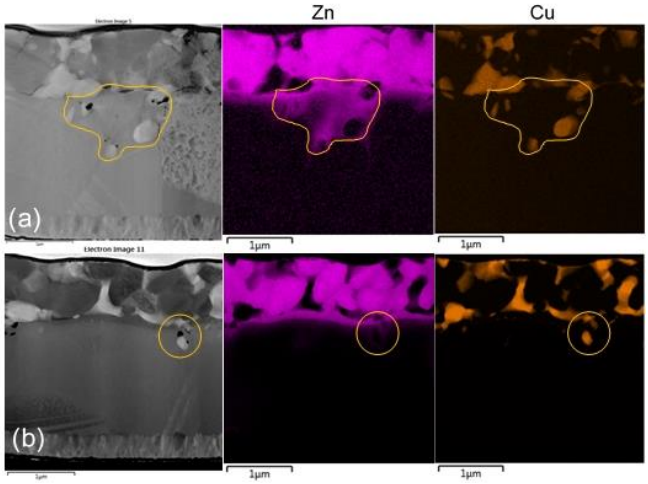

FIG. 8 (Color Online). TEM images and associated elemental maps from the identical sample (8% Cu, fully annealed) from a region a) containing defects due to the presence of several Cu_xTe clusters and b) a region with no grain boundaries and a single Cu_xTe cluster. Cluster regions outlined for clarity.

To confirm the critical role of morphology, additional experiments were performed using CdTe layers that were not subjected to $CdCl_2$ treatment prior to ZnTe:Cu deposition. As-deposited CdTe films exhibit much smaller grain sizes and are highly defective with numerous stacking faults.[11] Consistent with expectation the degree of interdiffusion was substantially enhanced in these bilayers. Figure 9 provides a comparison of XRD patterns for samples annealed at 360 ºC for 5 min using CdTe with and without $CdCl_2$ treatment as a function of Cu loading. No peak shift, hence negligible interdiffusion, is seen for the samples without Cu. The degree of interdiffusion is much more pronounced for the non-$CdCl_2$ samples with Cu present. It is well known that $CdCl_2$ treatment removes defects and improves CdTe crystallinity.[11,14] The relative disorder of non-treated films makes it easier for diffusion to occur. Interdiffusion is again most pronounced for the lowest Cu loading of 3%. Significant shifts occur for both CdTe and ZnTe peaks in contrast to $CdCl_2$ treated films, where no movement of CdTe peaks was observed. In addition, the area between CdTe and ZnTe peaks is noticeably above the background and the CdTe peak is strongly attenuated.

The intediffusion asymmetry observed in this work is in part supported by thermodynamics. Since CdTe and ZnTe share the same zinc blende crystal lattice it is often assumed that these compounds are fully miscible, and indeed they are at elevated temperatures (> 900 K). However, analysis of the vapor pressure composition above $Cd_xZn_{1-x}Te$ alloys indicated that the activity of ZnTe has a positive deviation from

ideality and conversely the activity of CdTe exhibits a negative deviation.[25] This non-ideal behavior is rare in solid solutions and means that that the addition of Cd to ZnTe results in just a small loss of ZnTe activity whereas the activity of CdTe is significantly attenuated upon Zn addition. In addition, vapor pressure data at T = 780 K suggests the presence of a miscibility gap in $Cd_xZn_{1-x}Te$ for $0.4 < x < 0.75$.[25] The asymmetry of this range and the activity behavior are both consistent with the idea that Cd solubility is ZnTe is greater than that of Zn in CdTe, consistent with our observations. The results described here are consistent with recent molecular dynamics (MD) simulations of this interface.[26] Using a Stillinger-Weber potential[27] these authors confirmed that Cd diffusion into ZnTe is much more extensive than Zn into CdTe, as well as the importance of structural defects to promote the latter. The MD simulations also confirmed that the presence of Cu enhanced interdiffusion.

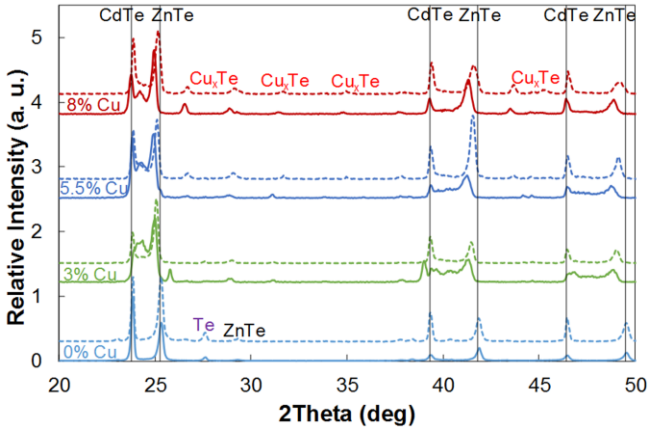

FIG. 9 (Color Online). XRD patterns of bilayers as a function of copper loading after t= 5 minutes of annealing at T = 360 ºC. Solid line: as-deposited CdTe, dashed: $CdCl_2$ treated.

C. Role of Copper on ZnTe Morphology and Cu_xTe Cluster Formation

The amount of copper present was found to have a profound impact on the morphology of the ZnTe layer and of course the formation of Cu_xTe clusters. In addition to facilitating interdiffusion, the presence of Cu promotes grain growth and has a densifying effect on the ZnTe layer. Figure 10 compares the cross-sectional TEM images of post 360°C 5 min RTP for all Cu loadings. There are numerous voids that can be seen in the 0% Cu sample represented by white spots in this bright field image. The void density is significantly attenuated for the 3% Cu sample along with a dramatic increase in the average ZnTe grain size. The average grain size continues to increase with the higher Cu loading, with grains reaching sizes of ~500 nm for the 8% sample. To illustrate this progression, a few of the grains are outlined in red in Fig. 10. The addition of Cu improves the stoichiometry of this layer. As mentioned previously the as-deposited ZnTe is Te rich, and EDAX line scans show that the 3% Cu sample contains regions with up to 20% excess Te as evidenced by the II/VI ratio. In contrast, the II/VI ratio is nominally unity throughout the 8% annealed sample since all excess Te is scavenged by Cu forming Cu_xTe.

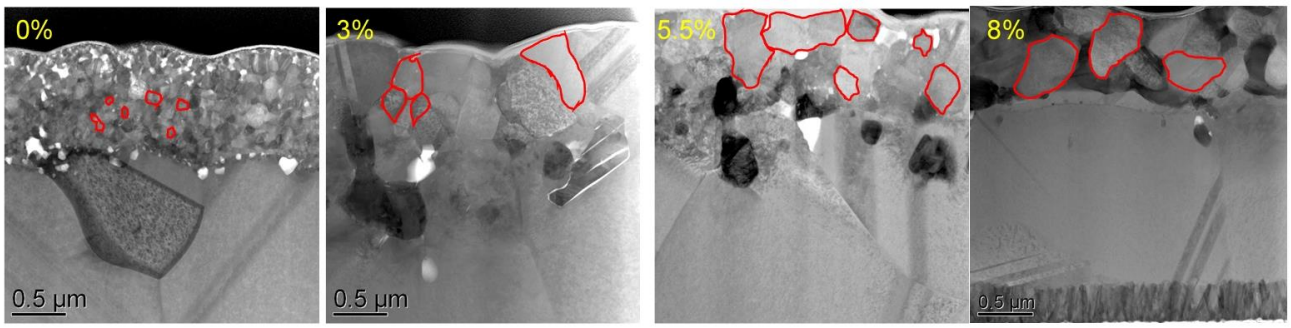

FIG. 10 (Color Online). Bright field TEM of post 360°C, 5 min RTP. Some grains are outlined for comparison.

Copper loading also impacts the identity of the phases of the Cu_xTe that are formed during annealing. Figure 11 displays an expanded view of the XRD region

associated with Cu_xTe phases as a function of Cu loading and annealing time at 360 ºC. The as-deposited 3% Cu sample has only one small peak around 37.6^o that could not be identified as any specific phase of Cu_xTe. As deposited samples for 5.5 and 8% Cu exhibit peaks that correspond to $Cu_{2.72}Te_2$. Annealing for just 30 seconds creates a significant redistribution of the minority phases in these bilayers. In the case of 3% Cu we observe the appearance of a Te peak, whereas for 5.5% Cu a small peak corresponding to CuTe is observed. More dramatic recrystallization is seen for 8% Cu loading where $Cu_{1.4}Te$ and Cu_2Te peaks appear. As the cumulative annealing time is increased to 2 and then 5 min, a blend of $Cu_{1.4}Te$ and Cu_2Te peaks are observed for 5.5 and 8% Cu samples, whereas the 3% Cu sample exhibits peaks corresponding to CuTe, Cu_4Te_3, and $Cu_{2.72}Te_2$. Identifying Cu_xTe can be challenging due to a wide variety of possible phases that it can form.[28] Nevertheless, the common trend observed is that as the level of Cu loading increases the resulting Cu_xTe phases become increasingly Cu-rich. This is similar to what has been observed in the devices contacted with Cu in the absence of ZnTe.[29] EDAX analysis of Cu_xTe clusters from fully annealed samples confirmed these trends, with 3% sample having Cu/Te ratios of 1-1.36, and 5.5 and 8% samples having Cu/Te ratios of 1.3-1.5 with some clusters reaching a value of ~2. In addition, data suggests that Cu loading rather than annealing temperature and time has a more profound effect on the identity of Cu_xTe phases that are formed. In our devices, the Cu loading is optimized for different metallization layers.[13] The performance optimization is dependent on the RTP temperature and time. Therefore, this seems to suggest that the degree of interdiffusion rather than specific Cu_xTe phase has a more significant effect on the cell performance of RTP-activated devices with ZnTe:Cu back contact.

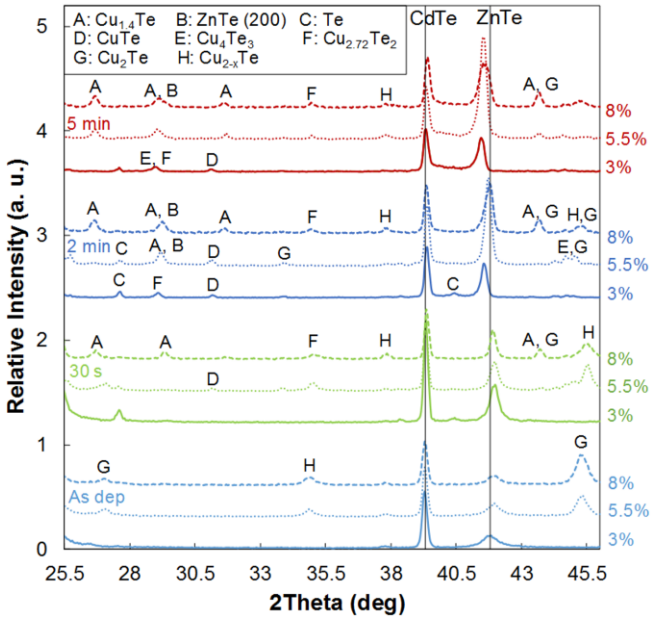

FIG. 11 (Color Online). XRD of 3, 5.5, and 8 vol% Cu samples annealed at 360 ^{o}C showing different phases of Cu_xTe complexes. For each annealing time on the graph, Cu vol% is increasing from bottom to top (solid to dashed line).

Time and temperature had a minor impact on Cu_xTe composition, but significantly impacted the migration and size of the clusters. Figure 12 below shows EDAX maps of 5.5% samples annealed for 5 minutes at temperatures of 320, 340, and 360 ^{o}C as well as of as-deposited sample. Prior to annealing, Cu is evenly distributed throughout the ZnTe layer. After RTP, copper is segregated into Cu_xTe clusters ranging in size from 10 to several hundred nm. These clusters are well correlated with the voids observed in the Zn and Cd elemental maps. The yellow lines in the figure are added to highlight the interface between ZnTe and CdTe layers. At 320 ^{o}C Cu_xTe clusters are initially confined within ZnTe layer with only a small fraction moving past the interface. As temperature increases, Cu_xTe coalesce into larger clusters, with some reaching ~1 μm in size. In addition, the clusters migrate into the CdTe, and at 360 ^{o}C the majority of clusters are inside the CdTe layer. These images also confirm our previous observations

of Cd-Zn interdiffusion. Cd appears to be distributed fairly uniformly throughout the entirety of ZnTe layer (excluding Cu_xTe clusters), which is clearly seen for the sample annealed at 360 ºC. In contrast, the extent of Zn diffusion into CdTe is relatively limited and predominantly associated with Cu_xTe clusters. As reported previously,[9] the Cu_xTe clusters are surrounded by Zn. Here we see that the Cu_xTe clusters seem to provide a preferred path for the movement of Zn into CdTe.

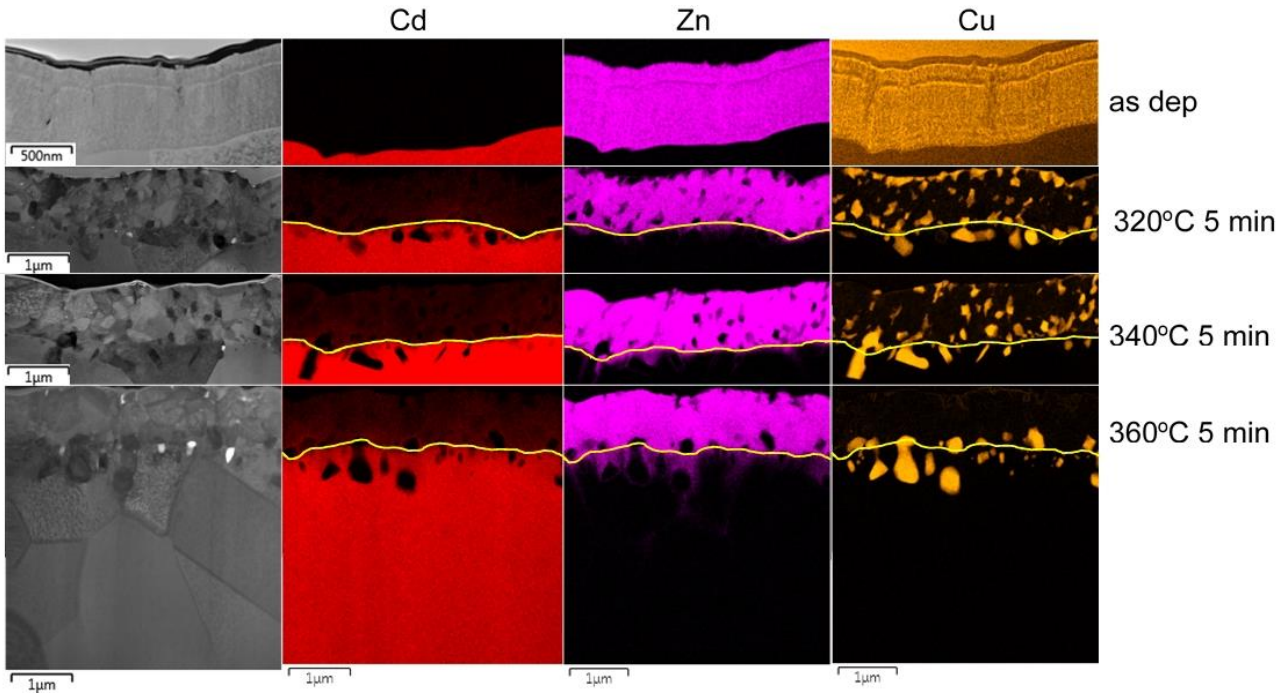

FIG. 12 (Color Online). TEM and EDAX maps of 5.5% sample as deposited and after annealing for 5 min at temperatures of 320, 340, and 360 ºC showing the coalescence and movement of Cu_xTe clusters. Yellow lines delineate the interface between CdTe and ZnTe.

D. Discussion

In the absence of Cu, temperatures of 475-550 ºC are required to induce the intermixing of CdTe and ZnTe thin films.[30] The results presented here show that copper

is an effective flux agent, catalyzing significant interdiffusion at temperatures of 320-360 ºC in a matter of minutes. This implies that in addition to its well documented role as a dopant in CdTe,[31,32] copper is essential to form a high quality CdTe|ZnTe interface under the conditions employed for back contact activation. As such, the presence of Cu is analogous to the role of $CdCl_2$ at the heterojunction region. Without $CdCl_2$, negligible CdS-CdTe interdiffusion occurs while in its presence CdS_yTe_{1-y} alloys are formed that approach solubility limits.[11,33] The importance of Cu is reinforced by the energetics, as the apparent activation energy for CdTe-ZnTe interdiffusion is comparable to the value for Cu interdiffusion. The prevalence of Cd to interdiffuse more rapidly into ZnTe than Zn into CdTe is consistent with thermodynamic and MD simulations. In addition, the role of microstructure and excess Te are also major contributors.

Another finding of this paper is the effect of copper on the morphology of ZnTe. Several researchers saw the structural quality of ZnTe degrade when doping with N_2.[19,34] Similarly Barati et. al.[35] had to use substrate temperatures of 420 ºC to achieve good crystallinity for low resistivity films when doping with Sb. In contrast to these group V dopants, copper appears to have a beneficial impact on ZnTe crystallinity and morphology. First, the intrinsic ZnTe films evaporated in this study contain excess Te. The presence of Cu during co-evaporation scavenges this excess Te. After annealing, TEM images show that ZnTe films containing copper have much larger crystals and fewer voids, attributed to copper's role of enhancing mobility. Larger grains would be beneficial to the device performance due to improved mobility. This could explain why good device performance is observed even when using substrate temperatures as low as 100 ºC for ZnTe:Cu deposition.[8]

One of the proposed roles of ZnTe layer in a CdTe solar cell is to act as an electron reflector at the back due to significant conduction band offset with CdTe.[36] In addition, interdiffusion of CdTe-ZnTe has been suggested to be essential for the formation of good ohmic contact in CdTe-based solar cells.[9] This interdiffusion would lead to formation of a graded junction, passivating the interface defects and lowering the stress caused by lattice mismatch of CdTe and ZnTe.[37] However, too much interdiffusion would defeat the purpose of electron reflection. It is shown here that the extent of interdiffusion varies with Cu loading, RTP temperature and treatment time. Therefore, these findings on the role of Cu in facilitating interdiffusion between CdTe and ZnTe provide an insight into optimization of device performance.

The aforementioned role of Cu in improving ZnTe crystal quality of ZnTe could potentially be applied in the synthesis of CZT absorbers. It has been reported that CZT alloys exposed to $CdCl_2$ experience incomplete recrystallization and void formation in addition to Zn loss.[38] Depositing Cu and ZnTe onto $CdCl_2$-treated CdTe and further annealing could be a novel way of preparing CZT absorbers. However, Cu loading would need to be minimized to avoid the formation of recombination centers. The Cu loadings explored here would be too high for that application. Due to limitations of the rate control in co-evaporation process, 3% loading is approaching the lower limit of what we can accurately measure with the current set-up. It would be valuable to explore the effects of Cu loading in the 0-3% range and apply those findings to both performance optimization and CZT synthesis.

IV. CONCLUSIONS

In this paper we present a study on the effect of Cu loading on the interdiffusion and recrystallization of CdTe/ZnTe thin films. It was found that Cu facilitates interdiffusion between CdTe and ZnTe, and that negligible interdiffusion occurs under back contact activation conditions in the absence of copper. Increasing treatment time and temperature increases the extent of interdiffusion, whereas interdiffusion was maximized at the lowest copper loading. Elemental mapping shows that Cd moves into ZnTe and is fairly uniformly distributed. Zn migration into CdTe is limited to regions containing defects or through its association with migrating Cu_xTe clusters. Copper scavenges excess Te and leads to improved crystallinity, grain size, and morphology in the annealed films. The composition of Cu_xTe clusters mostly depends on Cu loading, while their size and migration are dependent on annealing conditions.

ACKNOWLEDGMENTS

The CSM authors are grateful to the National Science Foundation through award number CBET-1706149.The Loughborough authors are grateful to UKERC for funding this work through the EPSRC Supergen SuperSolar Hub, grants EP/J017361/1 and EP/M014797/1.

[1]M. A. Green, K. Emery, Y. Hishikawa, W. Warta, E. D. Dunlop, D. H. Levi, and A. W. Y. Ho-Baillie, Prog. Photovoltaics **25,** 3 (2017).

[2]A. L. Fahrenbruch, Mater. Res. Soc. Symp. Proc. **1012,** 283 (2007).

[3]T. A. Gessert, A. R. Mason, P. Sheldon, A. B. Swartzlander, D. Niles, and T. J. Coutts, J. Vac. Sci. Technol. A **14,** 806 (1996).

[4]B. E. McCandless and K. D. Dobson, Solar Energy **77,** 839 (2004).

[5]N. Strevel, L. Trippel, C. Kotarba, and I. Khan, Photovoltaics International **22,** 66 (2014).

[6]C. W. Warren, J. Li, C. A. Wolden, D. M. Meysing, T. M. Barnes, D. W. Miller, J. T. Heath, and M. C. Lonergan, Appl. Phys. Lett. **106,** 203903 (2015).

[7]S. H. Demtsu, D. S. Albin, J. R. Sites, W. K. Metzger, and A. Duda, Thin Solid Films **516,** 2251 (2008).

[8]J. Li, D. R. Diercks, T. R. Ohno, C. W. Warren, M. C. Lonergan, J. D. Beach, and C. A. Wolden, Sol. Energy Mater. Sol. Cells **133,** 208 (2015).

[9]C. A. Wolden, A. Abbas, J. Li, D. R. Diercks, D. M. Meysing, T. R. Ohno, J. D. Beach, T. M. Barnes, and J. M. Walls, Sol. Energy Mater. Sol. Cells **147,** 203 (2016).

[10]A. Abbas, D. M. Meysing, J. Li, J. D. Beach, T. M. Barnes, J. M. Walls, and C. A. Wolden, in *Structural and chemical characterization of the back contact region in high efficiency CdTe solar cells*, 2015, p. 1.

[11]B. E. McCandless, L. V. Moulton, and R. W. Birkmire, Prog. Photovolt.: Res. Appl. **5,** 249 (1997).

[12]A. Abbas, G. D. West, J. W. Bowers, P. Isherwood, P. M. Kaminski, B. Maniscalco, P. Rowley, J. M. Walls, K. Barricklow, W. S. Sampath, and K. L. Barth, IEEE J. Photovoltaics **3,** 1361 (2013).

[13]J. Li, T. R. Ohno, and C. A. Wolden, in *The impact of different metallization layers on CdTe solar cells contacted with ZnTe:Cu buffer layers*, 2016, p. 1474.

[14]H. R. Moutinho, J. Vac. Sci. Technol. A **16,** 1251 (1998).

[15]R. D. Feldman, R. F. Austin, P. M. Bridenbaugh, A. M. Johnson, W. M. Simpson, B. A. Wilson, and C. E. Bonner, J.Appl. Phys. **64,** 1191 (1988).

[16]G. K. Rao, K. V. Bangera, and G. K. Shivakumar, Vacuum **83,** 1485 (2009).

[17]B. Späth, J. Fritsche, A. Klein, and W. Jaegermann, Appl. Phys. Lett. **90,** 062112 (2007).

[18]B. E. McCandless, M. G. Engelmann, and R. W. Birkmire, J. Appl. Phys. **89,** 988 (2001).

[19]A. E. Rakhshani, Thin Solid Films **536,** 88 (2013).

[20]P. M. Borsenberger and D. A. Stevenson, J. Phys. Chem. Solids **29,** 1277 (1968).

[21]R. A. Reynolds and D. A. Stevenson, J. Phys. Chem. Solids **30,** 139 (1968).

[22]T. D. Dzhafarov, S. S. Yesilkaya, N. Yilmaz Canli, and M. Caliskan, Sol. Energy Mater. Sol. Cells **85,** 371 (2005).

[23]H. H. Woodbury and M. Aven, J. Appl. Phys. **39,** 5485 (1968).

[24]E. D. Jones, N. M. Stewart and J. B. Mullin, J. Cryst. Growth **117,** 244 (1992).

[25]A. S. Alikhanian, V. N. Guskov, J. H. Greenberg, M. Fiederle, and K. W. Benz, J. Alloys Compd. **371,** 82 (2004).

[26]R. Aguirre, J. J. Chavez, J. Li, X. W. Zhou, S. F. Almeida, C. Wolden, and D. Zubia, IEEE J. Photovoltaics **8,** 594 (2018).

[27]X. W. Zhou, D. K. Ward, J. E. Martin, F. B. van Swol, J. L. Cruz-Campa, and D. Zubia, Phys. Rev. B **88** (2013).

[28]A. S. Pashinkin and V. A. Fedorov, Inorg. Mater. **39,** 539 (2003).

[29]X. Wu, J. Zhou, A. Duda, Y. Yan, G. Teeter, S. Asher, W. K. Metzger, S. Demtsu, S.-H. Wei, and R. Noufi, Thin Solid Films **515,** 5798 (2007).

[30]R. Dhere, T. Gessert, J. Zhou, J. Pankow, S. Asher, and H. Moutinho, Phys. Status Solidi B **241,** 771 (2004).

[31]L. Kranz, C. Gretener, J. Perrenoud, R. Schmitt, F. Pianezzi, F. La Mattina, P. Blosch, E. Cheah, A. Chirila, C. M. Fella, H. Hagendorfer, T. Jager, S. Nishiwaki, A. R. Uhl, S. Buecheler, and A. N. Tiwari, Nat. Commun. **4,** 2306 (2013).

[32]J. D. Poplawsky, N. R. Paudel, C. Li, C. M. Parish, D. Leonard, Y. Yan, and S. J. Pennycook, Adv. Energy Mater. **4,** 1400454 (2014).

[33]B. E. McCandless, G. M. Hanket, D. G. Jensen, and R. W. Birkmire, J. Vac. Sci. Technol. A **20,** 1462 (2002).

[34]T. M. Shimpi, J. Drayton, D. E. Swanson, and W. S. Sampath, J. Electron. Mater. **46,** 5112 (2017).

[35]A. Barati, A. Klein, and W. Jaegermann, Thin Solid Films **517,** 2149 (2009).

[36]B. Späth, J. Fritsche, F. Säuberlich, A. Klein, and W. Jaegermann, Thin Solid Films **480-481,** 204 (2005).

[37]Y. H. Kim, I. J. Kim, S. D. Lee, K. N. Oh, S. K. Hong, S. U. Kim, M. J. Park, J. Cryst. Growth **214/215,** 225 (2000).

[38]T. M. Shimpi, J. M. Kephart, D. E. Swanson, A. H. Munshi, W. S. Sampath, A. Abbas, and J. M. Walls, J. Vac. Sci. Technol. A **34,** 051202 (2016).

FIGURE CAPTIONS

FIG. 1 (Color Online). XRD patterns of CdTe|ZnTe bilayers obtained from as-deposited films (solid lines) and after full annealing (T = 360 ºC, t= 5 min, dashed lines) as a function of copper loading.

FIG. 2 (Color Online). Comparison of TEM images and elemental EDAX maps after annealing at T = 360 ºC for a cumulative time of t = 5 min: a) 0 % Cu; b) 3% Cu.

FIG. 3 (Color Online). XRD patterns from the 5.5 vol% Cu sample annealed at 320, 340, and 360 ^{o}C after 0.5, 2, and 5 minutes of cumulative annealing.

FIG. 4 (Color Online). CdxZn1-xTe alloy composition as function of annealing time, Cu loading, and annealing temperature based on analysis of the ZnTe (220) peak position: a) 320 ^{o}C; b) 340 ^{o}C; c) 360 ^{o}C

FIG. 5 (Color Online). Arrhenius plot of $Cd_xZn_{1-x}Te$ alloy compositions based on analysis of the ZnTe (220) peak position of samples annealed for 5 min.

FIG. 6 (Color Online). a) Cd and Zn profiles from EDAX line scans in 3% and 8% samples annealed at 360 ^{o}C for 5 min; b) line scan position for 3% Cu sample; c) line scan position for 8% Cu sample.

FIG. 7 (Color Online). a) TEM images with the region of area scans highlighted; b) average concentrations of Cd in 1 micron of ZnTe layer and Zn in 1 micron of CdTe calculated from EDAX line scans; c) concentrations of Cd and Zn obtained from the selected area scans shown in (a).

FIG. 8 (Color Online). TEM images and associated elemental maps from the identical sample (8% Cu, fully annealed) from a region a) containing defects due to the presence of several Cu_xTe clusters and b) a region with no grain boundaries and a single Cu_xTe cluster. Cluster regions outlined for clarity.

FIG. 9 (Color Online). XRD patterns of bilayers as a function of copper loading after t= 5 minutes of annealing at T = 360 ºC. Solid line: as-deposited CdTe, dashed: $CdCl_2$ treated.

FIG. 10 (Color Online). Bright field TEM of post 360^{o}C, 5 min RTP. Some grains are outlined for comparison.

FIG. 11 (Color Online). XRD of 3, 5.5, and 8 vol% Cu samples annealed at 360 ^{o}C showing different phases of Cu_xTe complexes. For each annealing time on the graph, Cu vol% is increasing from bottom to top (solid to dashed line).

FIG. 12 (Color Online). TEM and EDAX maps of 5.5% sample as deposited and after annealing for 5 min at temperatures of 320, 340, and 360 ºC showing the coalescence and movement of Cu_xTe clusters. Yellow lines delineate the interface between CdTe and ZnTe.